SUPPORTING INFORMATION

Multi-stage Ensemble-learning-based Model Fusion for Surface Ozone Simulations: A Focus on CMIP6 Models

Authors

Zhe Sun[1,2*], Alexander T. Archibald[1,3*]

Affiliations

[1] Centre for Atmospheric Science, Yusuf Hamied Department of Chemistry, University of Cambridge, Cambridge CB2 1EW, UK

[2] Department of Earth Sciences, University of Cambridge, Cambridge CB2 3EQ, UK

[3] National Centre for Atmospheric Science, Cambridge CB2 1EW, UK

[*] Corresponding authors:
Zhe Sun (zs347@cam.ac.uk) and Alexander T. Archibald (ata27@cam.ac.uk)

21 pages, 13 figures, and 3 tables in total.

CMIP6 Surface O_3 historical simulation participant research institutes

The 13 research institutes are Alfred Wegener Institute (AWI), Beijing Climate Centre (BCC), the HAMMOZ-Consortium (consisting of Swiss Federal Institute of Technology Zurich, Max Planck Institute for Meteorology, Forschungszentrum Jülich, University of Oxford, Finnish Meteorological Institute, Leibniz Institute for Tropospheric Research and Centre for Climate Systems Modelling at ETH Zurich), Institute Pierre-Simon Laplace (IPSL), Met Office Hadley Centre (MOHC), Met Office Natural Environment Research Council (MO-NERC), Max Planck Institute for Meteorology (MPI-M), Japan Meteorological Research Institute (MRI), NASA Goddard Institute for Space Studies (NASA-GISS), National Centre for Atmospheric Research (NCAR), Norwegian Climate Centre (NCC), National Institute of Meteorological Sciences – Korea Meteorological Administration (NIMS-KMA), and the Geophysical Fluid Dynamics Laboratory of the National Oceanic and Atmospheric Administration (NOAA-GFDL).

Detailed annotations on atmospheric module settings

Multiple sub-experiments are noted with different chaotic climate realisations (r), initialisations (i), aerosol physics (p) and forcing (f). Reproducing the multicentury global-scale weather and climate conditions shall be crucial to the CCMs which have amalgamated the atmospheric component-climate interaction effects. However, the Earth climate is so complex and chaotic that it is rather difficult to simulate the decadal realistic climate system, past, present and future. In this sense, CMIP6 completed a series of experiments to realise the near-equilibrium pre-industrial state of the climate system as control (denoted as *piControl* in DECK),[1] starting from initial climate spin-ups centuries ago and gradually reaching balance with forcing by the selected starting year for the modelling of atmospheric components, as 1850 in this current study.[2]

Considering the butterfly effect in the climate system that small disturbances in temperature, wind, humidity and other weather features even in a small place will possibly lead to different future evolution paths of the whole climate system,[3] unique initial climate conditions are realised from different simulation starting dates with the same coupled model and same atmospheric physics. All these realisations are kept, as the simulation ensemble can be able to reproduce the weather events with similar frequency as observed records, and the initial climate conditions should also have fully represented the Interdecadal Pacific Oscillation[4-8] and the Atlantic Multidecadal Oscillation,[9-12] manifested by basin-scale variability in sea surface temperature (SST).[13, 14] In addition, these multiple unique but reasonable realisations can verify how the small disturbance in SST will affect the atmospheric chemistry processes. Though the individual ensemble members of initial climate simulations differed from each other, they are still of high similarity in a relatively longer time-scale, so that are all used for CMIP6 atmospheric historical simulations.[2, 15] The initialisation time point is consistently set as 1850 within the scope of this research, so that all the experiments are marked as i_1.

CMIP6 historical simulations consider 3 aerosol microphysics as the calculation of atmospheric compositions can be realised by non-interactive (NINT) read-in of pre-computed transient aerosol and ozone fields (p_1),[16] One-Moment Aerosol scheme (OMA, p_3) with the "Tracers, Chemistry, Aerosols Direct and Indirect Effect (TCADI)" configuration,[16, 17] and more complex Multi-configuration Aerosol TRacker of mIXing state (MATRIX, p_5),[16, 18] among which p_3 and p_5 considered cloud impacts. The major difference between the OMA and TOMAS is the calculation algorithm of the particle size distribution (PSD), in which the one-moment scheme will only involve the mass concentration while the two-moment scheme can consider both the mass and the number concentrations.[18-20] As p_5 can be regarded as an extended setting of p_4 without much more computation burdens, the CMIP6 historical and future scenario simulation experiments did not include p_4, so that comparisons will only be made between p_1, p_3, and p_5 within the scope of this current study, and till present (2021), different aerosol micro-physics configurations are only considered by NASA-GISS-E2.1 model series.

Three radiative forcing prescriptions are used and noted as f_1, f_2, and f_3. Pattern f_1 represents the compositional forcing derived from OMA simulations, based on which the ozone-related heterogeneous reactions are corrected into pattern f_2; f_3 is the same as f_2, except the stratospheric surface area density of aerosols (SAD) is fixed at 1850 values.

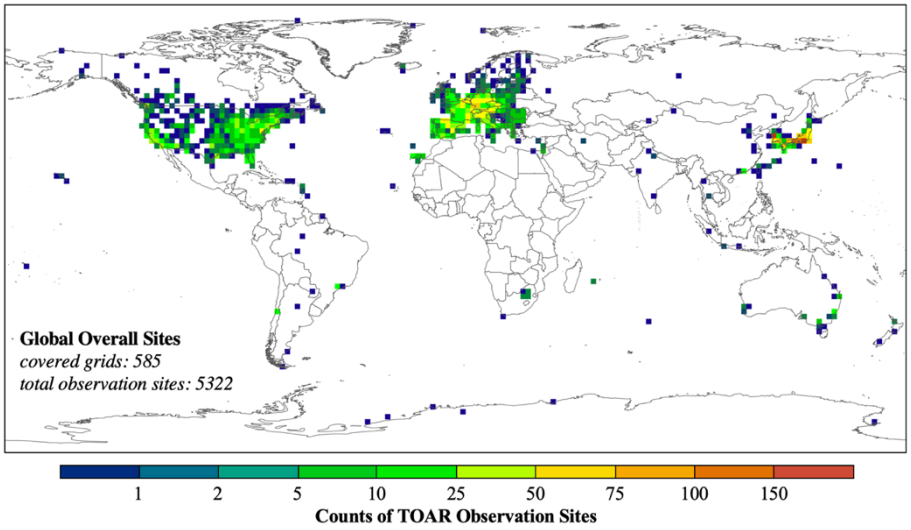

Figure S1 Global distribution of TOAR sites during 1990-2014. The TOAR ground monitoring sites are clustered into coordinational grids with 2°×2° spatial resolution, and the counts of observational sites in each grid are marked in different colours.

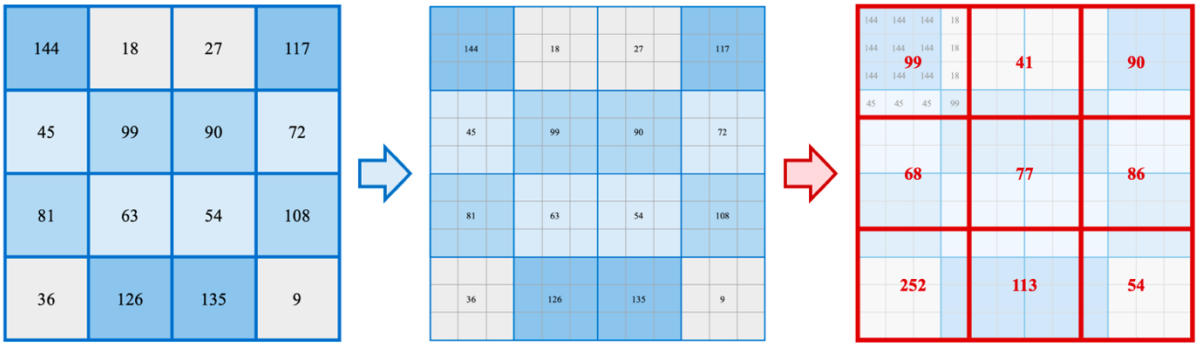

Figure S2 Schematic graph for re-gridding process. A faked dataset is used to illustrate the segmentation and re-aggregation process. During segmentation, interpolation is performed by deploying the same values of the larger grid for the spatial continuous variables (i.e. pollution concentrations), and using the equally distributed values for the discrete variables (i.e. population), so that during re-aggregation, values for the grids are calculated as average for continuous variables and sum for discrete variables correspondingly.

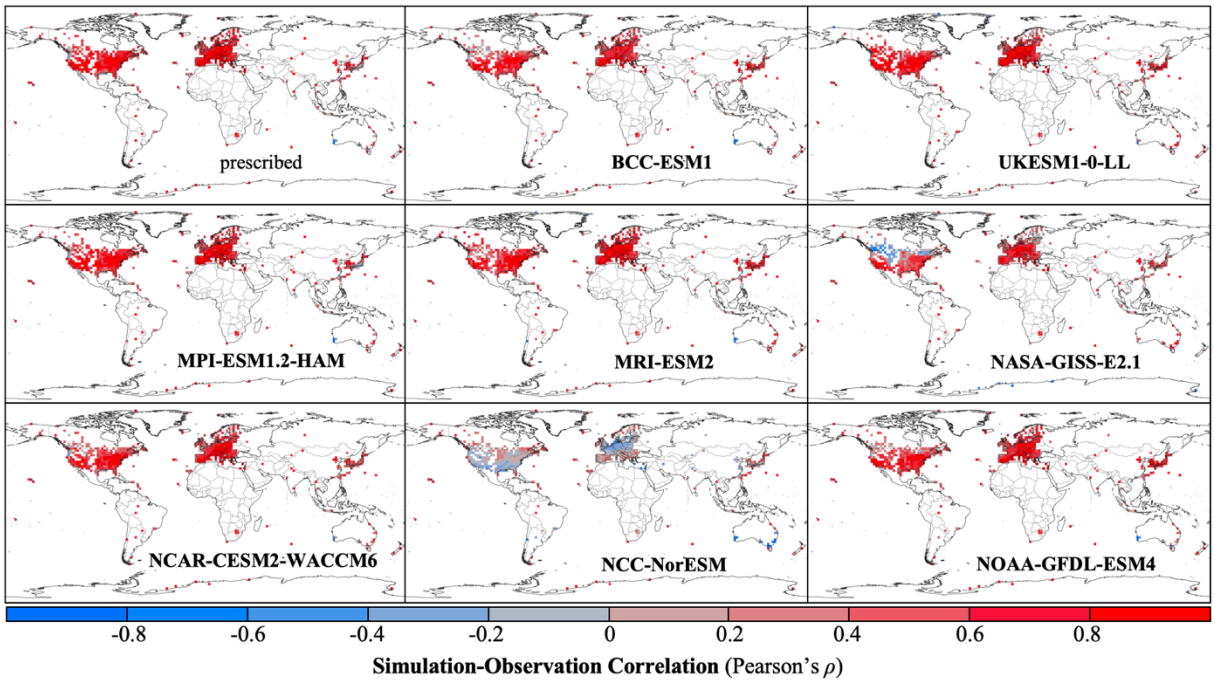

Figure S3 Correlation distributions between TOAR observations and CMIP6 multi-realisation-ensembled individual model simulations of surface ozone concentrations during 1990-2014. A total of 8 individual models together with the prescribed ozone are considered, and the grid-specific correlations are mapped onto all covered TOAR monitoring sites and scaled in blue-red colour bar where red spatial cells indicate higher positive correlations, the grey-coloured cells indicate failure in capturing the temporal variations of surface ozone concentrations, and blue-coloured cells refer to the reversed (negative) correlation between observations and simulations.

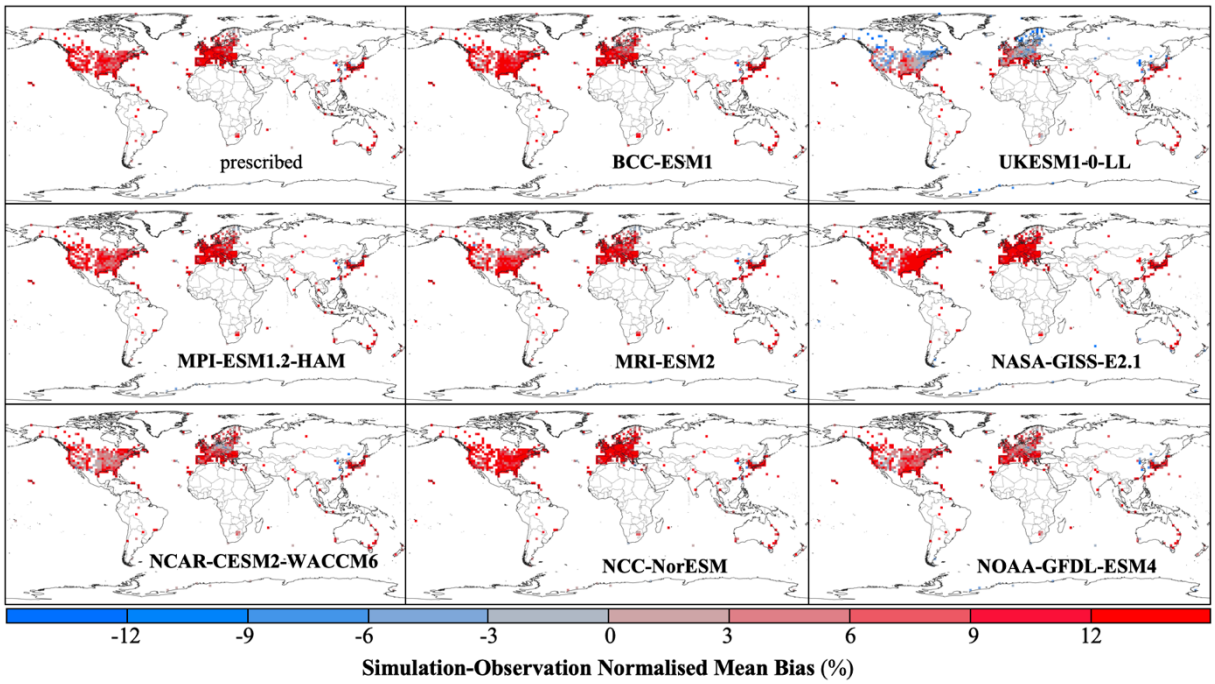

Figure S4 Global distributions of normalised mean biases between individual CMIP6 simulations and TOAR observations of surface ozone through 1990-2014. The normalised mean biases (NMB) are defined on the cell-specific 25-year full-duration (1990-2014) overall average concentrations for each individual model, mapped onto all covered TOAR monitoring sites with red-coloured cells indicating over-estimations and grey cells reflecting underestimations.

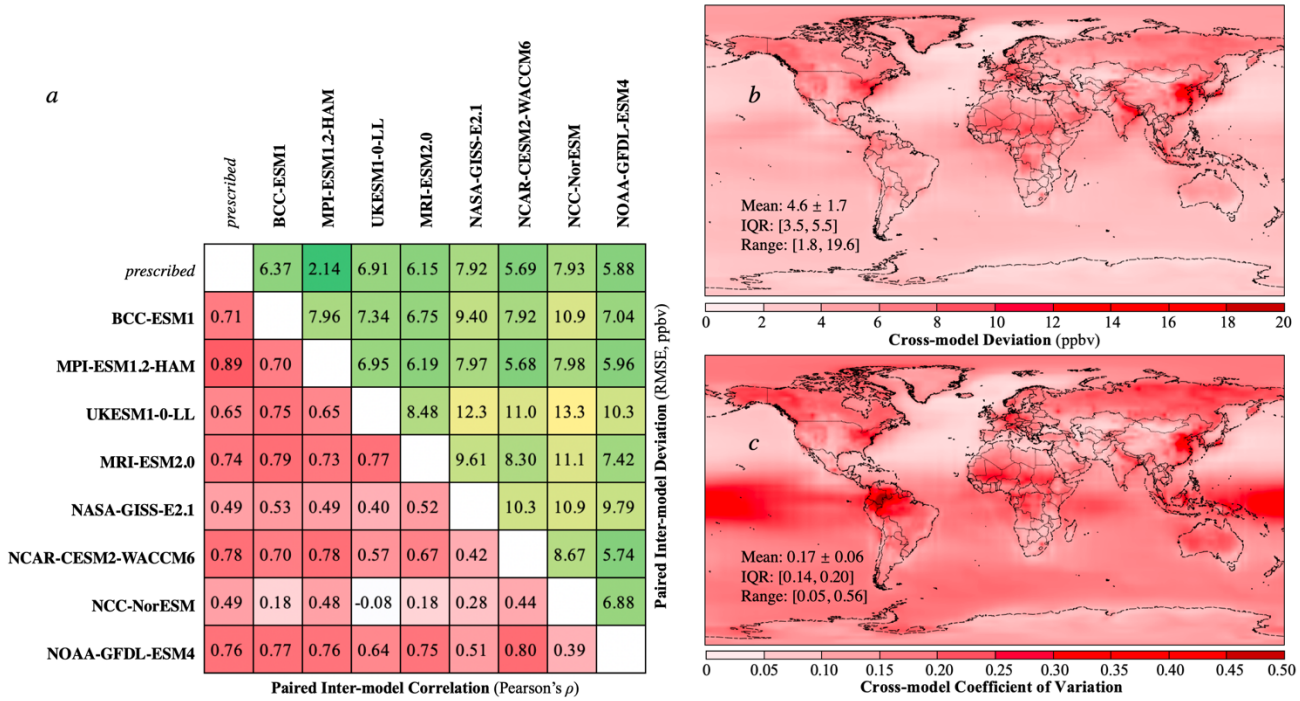

Figure S5 Inter-model similarity and divergence of CMIP6 simulation ensemble. The paired linear correlations defined as Pearson's ρ and biases quantified by root mean squared error (RMSE) were presented in lattice (panel *a*), where red correlations and green deviations representing higher similarity (i.e. higher Pearson's ρ and lower RMSE). The model-paired correlations and deviations are calculated upon the 9 multi-realisation ensemble average for the concision of summarisation, also owing to the high similarities across the realisations. The cross-model standard deviations through 1990-2014 are calculated from 58 individual simulations and mapped in panel *b*, with the relative deviations quantified in coefficient of variation (standard deviations divided by arithmetic mean) mapped in panel *c*.

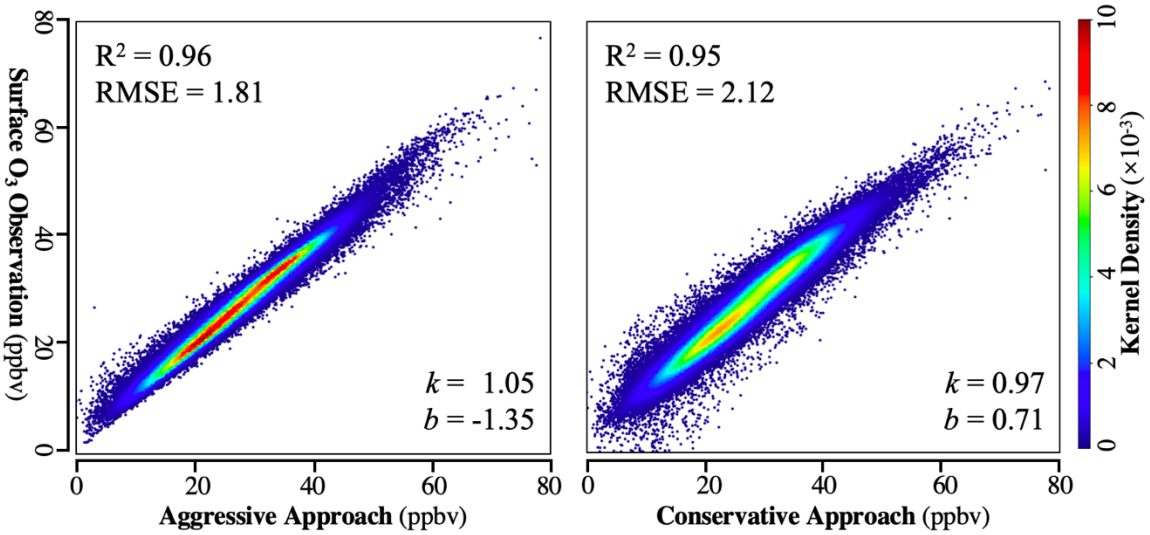

Figure S6 Model-observation evaluation for multi-model fusion by aggressive and conservative approach. Gaussian kernel density estimation is applied to construct the scatter plot. Evaluations are conducted on all observation covered regions and periods during 1990-2014. The overall R^2, RMSE, relative slope *k* and bias *b* are given for either multi-model fusion approach.

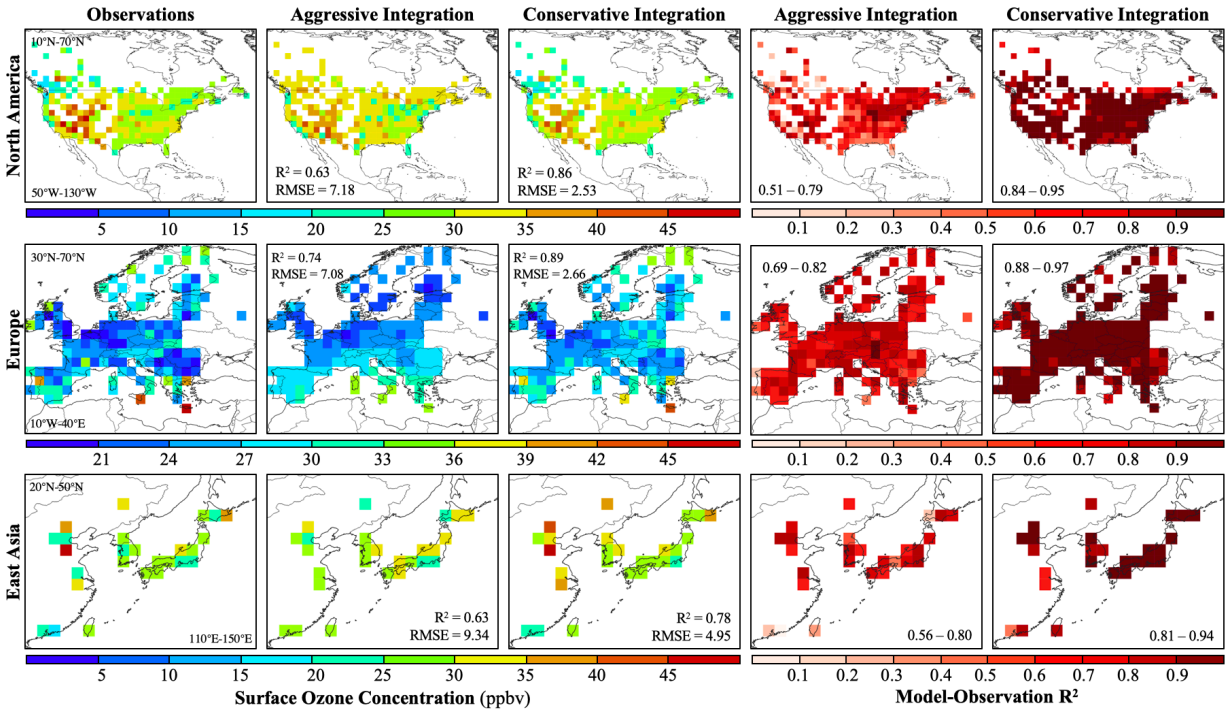

Figure S7 Regional extrapolation evaluation of aggressive and conservative multi-model ensemble integration. The spatial extrapolation experiments are conducted by 3 different training-*test* combinations, as Europe-*North America*, North America-*Europe*, and Western-*East Asia*. The first column presents the total average observed surface ozone concentrations measured by TOAR through 1990-2014. The second and third columns map the fused multi-model simulations by aggressive and conservative approaches, respectively, with the overall coefficient of determination (R^2) and root mean squared error (RMSE). The fourth and fifth columns quantify the spatial grid-specific model-observation fitting R^2 of aggressive and conservative approaches, respectively, indicated with the inter-quartile range (IQR). Overall, the conservative approach integrated performances for North America ($R^2 = 0.86$, RMSE = 2.53), Europe ($R^2 = 0.89$, RMSE = 2.66), and Asia ($R^2 = 0.78$, RMSE = 4.95) are better than aggressive approach integrated performances for North America ($R^2 = 0.63$, RMSE = 7.18), Europe ($R^2 = 0.74$, RMSE = 7.08), and Asia ($R^2 = 0.63$, RMSE = 9.34).

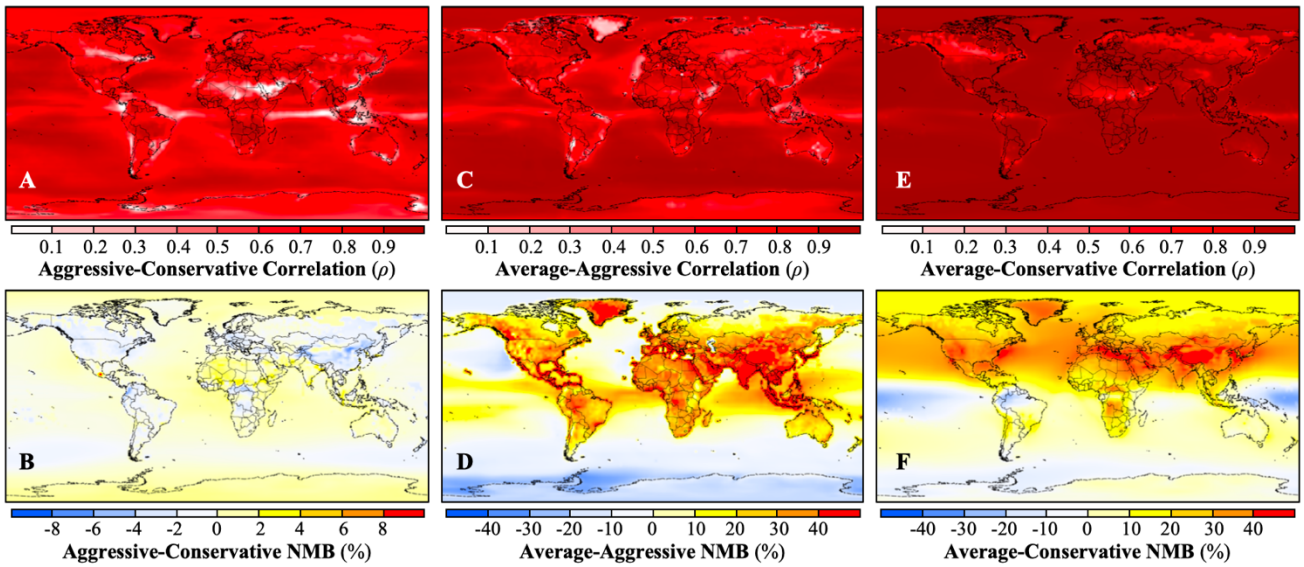

Figure S8 Similarity and discrepancy between 3 different multi-model ensemble approaches: arithmetic average, aggressive and conservative integration. The similarities are quantified as synchronicity by Pearson's correlation coefficient ρ; while the discrepancies are scaled by normalised mean bias (NMB, %). The statistics are drawn by inter-comparisons on 25-year ensembled surface ozone during 1990-2014, and summarised in average for mapping. The NMBs defined with $A - B$ are calculated as $\sum (A_i - B_i) / \sum B_i$, setting B as the reference.

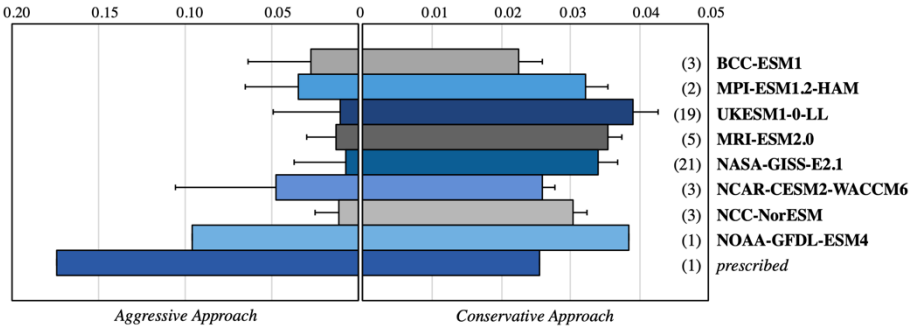

Figure S9 Individual model ensemble weights by aggressive and conservative integration approaches for 25-year simulation during 1990-2014. The 18 individual models were grouped into 4 major categories as non-interactive chemistry (NINT), UKESM1 chemistry schemes, NASA-GISS series, and other interactive chemistry driven models (INT-Chem). The weight uncertainties characterised by error bars of aggressive approach were estimated from different random seeds for ensemble learning model construction, while of conservative approach were given as the spatiotemporal variations instead, as the variability from Bayesian MCMC simulations were rather small. The weights presented in histogram referred to the model weights on TOAR covered locations, and the global weights given by Bayesian neural network regressions were also listed in the inserted columns.

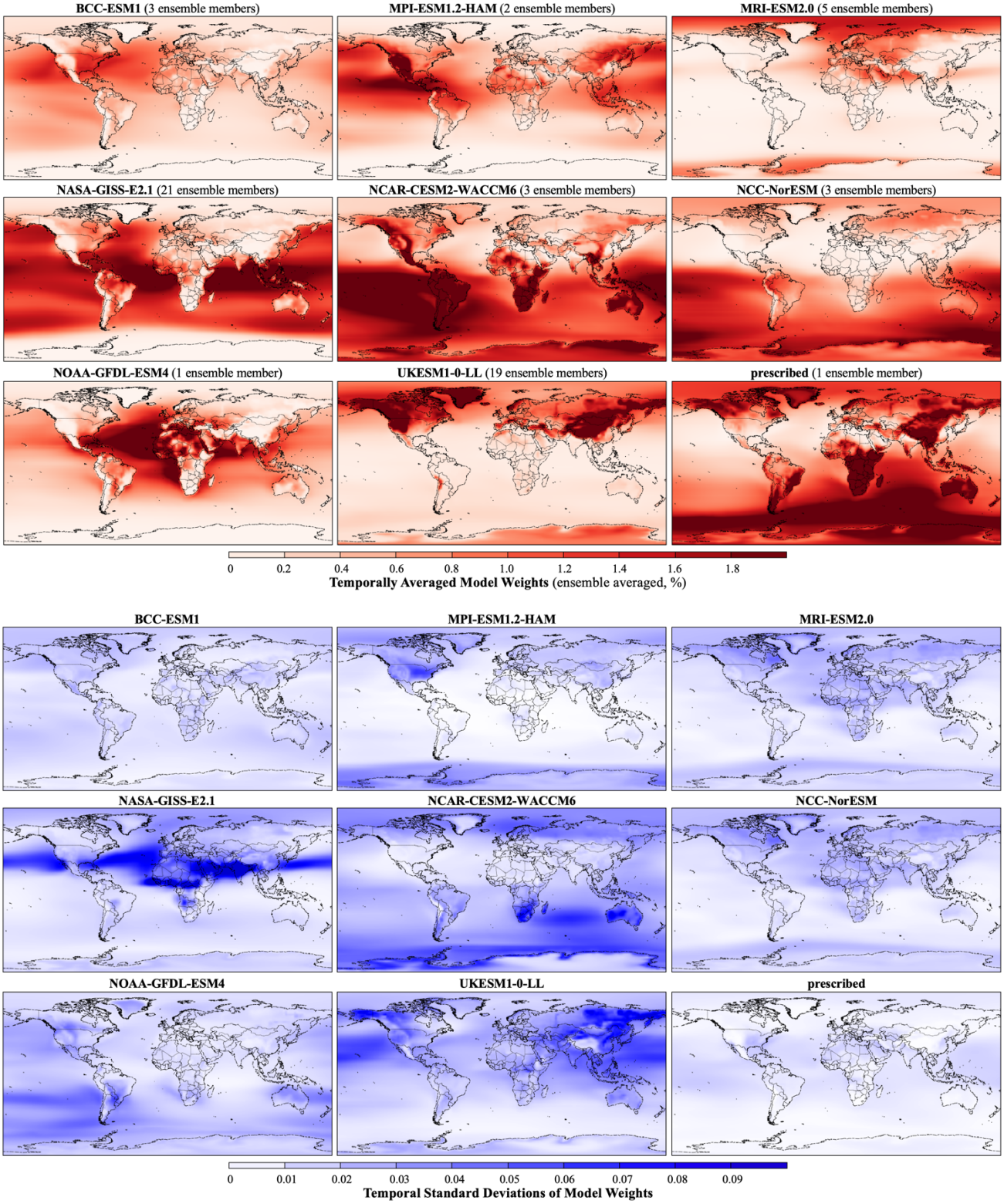

Figure S10 Temporal averaged global distribution of individual model weights by conservative space-time Bayesian neural network regression-based integration. The arithmetically averaged weights and standard deviations for linear combination of the 58 involved CMIP6 model simulation ensembles are calculated across 1990-2014, with darker reds indicating higher contribution weights and darker blue representing higher temporal variability. The spatial weights are also summarised as multi-realisation ensemble average for the concision of summarisation.

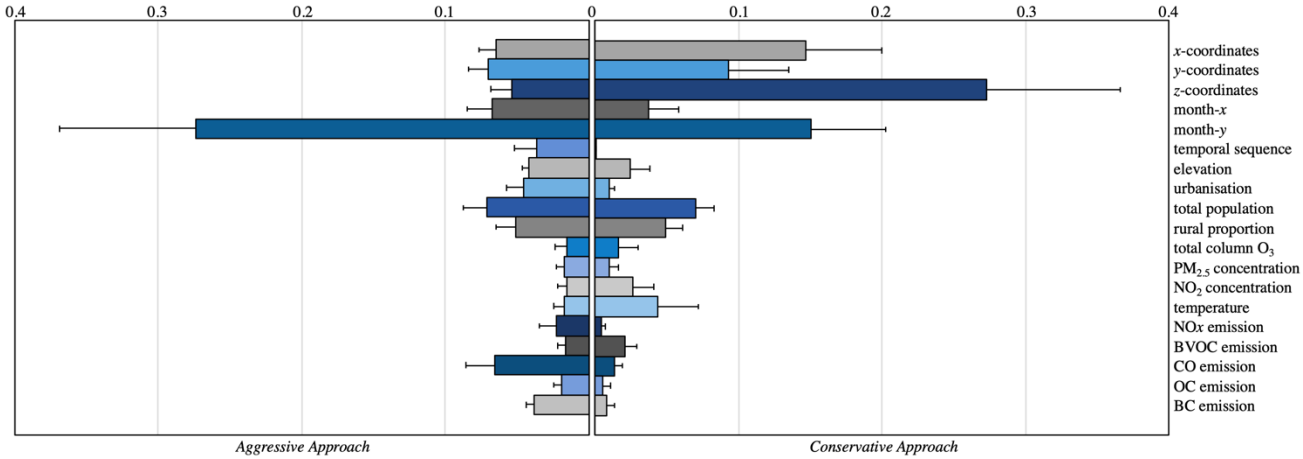

Figure S11 Contribution weights of additional assistant features for ensemble deep learning-based CMIP6 model prediction enhancement by aggressive and conservative multi-model integration approach. The weights are normalised by excluding the CMIP6 individual model contributions and shown in histograms with error bars representing the variations across different algorithms for aggressive approach and the spatiotemporal variability for conservative approach.

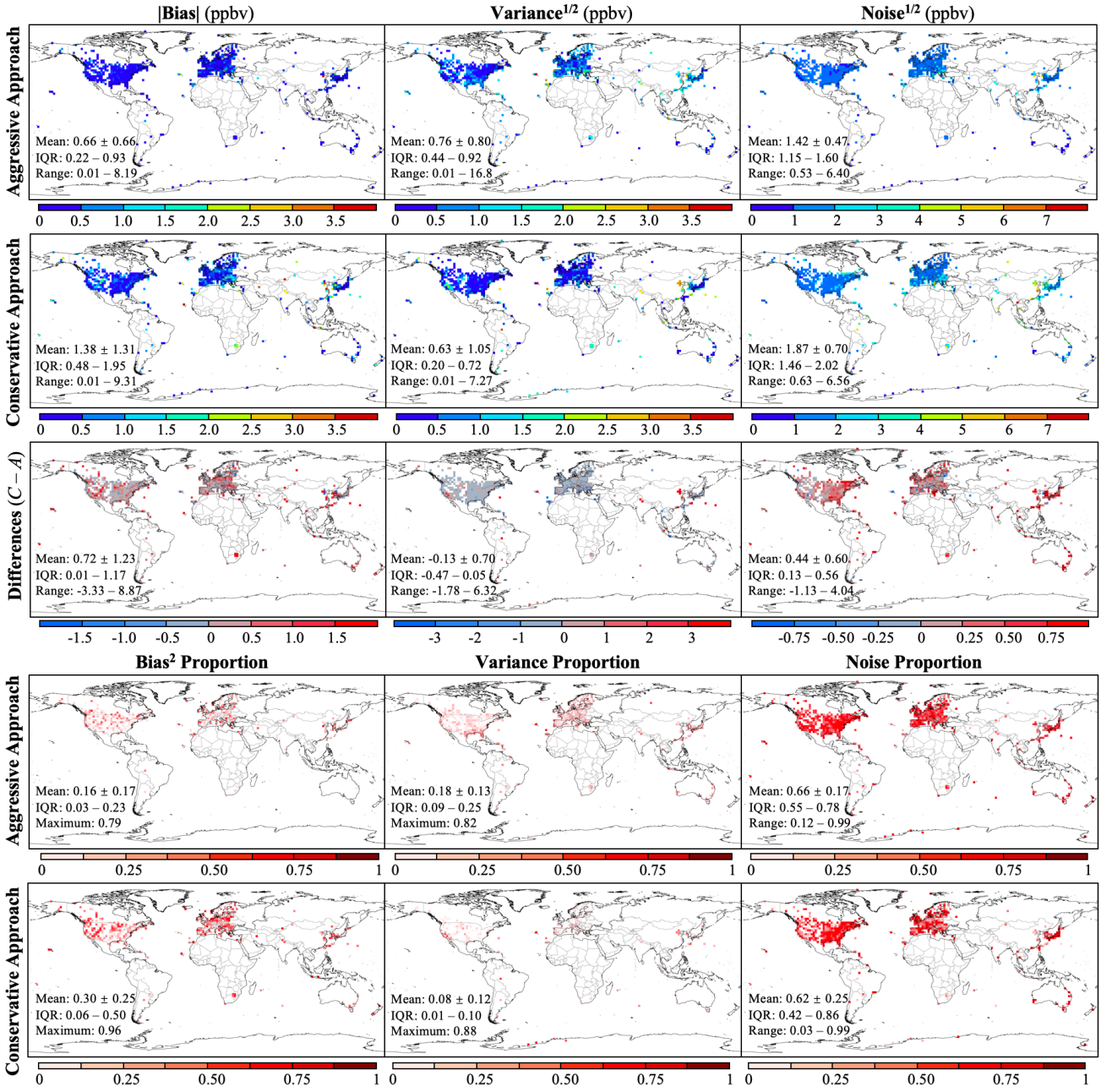

Figure S12 Decomposition of model-observation errors into bias, variance and noise in aggressive and conservative multi-model ensemble for surface ozone simulation. By definition, MSE = bias^2 + model variance + noise. Absolute values of bias, root variance and root noise for both aggressive and conservative approaches together with the differences, and the proportions of the squared bias, variance and noise are mapped individually. Major statistics include arithmetic mean, standard deviation, full range and inter-quartile range (IQR) are summarised for each metric. For the proportions of bias^2 and variance, the ranges are replaced by maximums, as the minimums are extremely small.

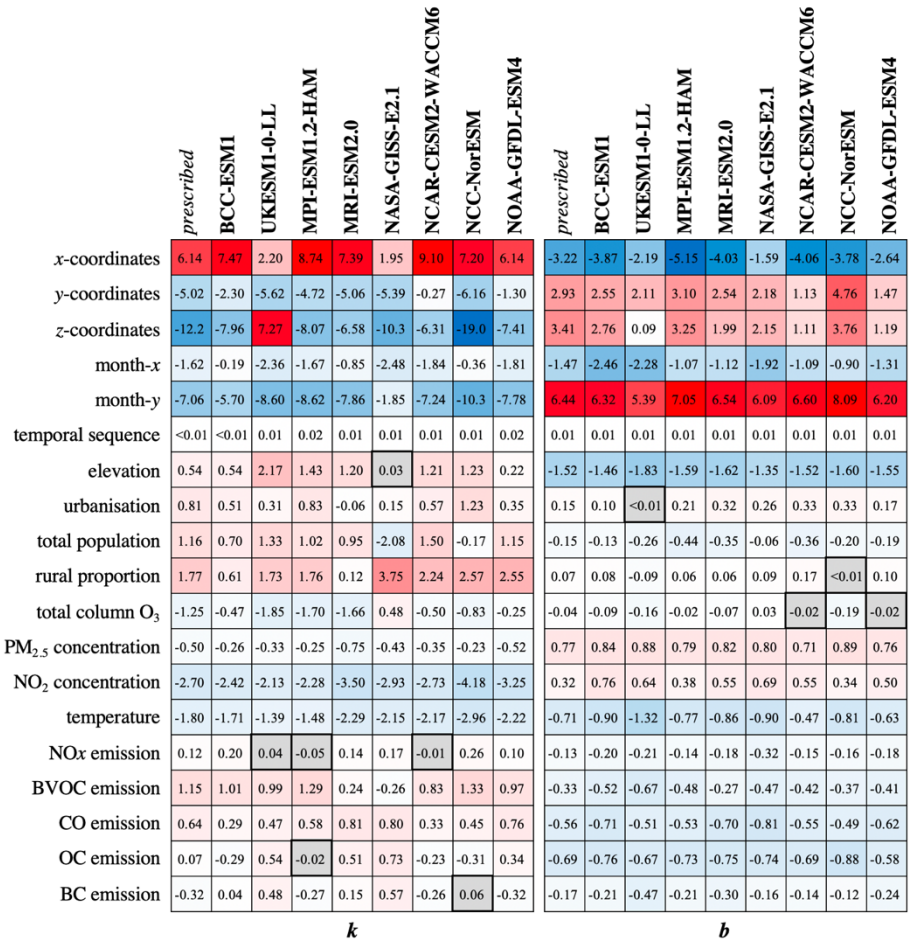

Figure S13 Correlation strength between the assistant features and single model calibration parameters by Bayesian neural network regression. The regressions are conducted on the standardised variables, with the left panel referring to the re-scaling parameter (slope *k*) and the right referring to the bias-correction parameter (intercept *b*). The values represent the regression coefficients, among which 10^{-2} is scaled for *k*. The positive correlations are shown in red while the negative correlations are in blue, with darker colours representing stronger associations. Grey cells indicate insignificant correlations.

Table S1 Summarisation of CMIP6 historical project participant institutes and models with chemistry schemes, spatial gridding, and experiment realisation, physics, and forcing scenarios. The names of institutes and coupled earth system models are listed in abbreviation. The three-dimensional spatial resolutions are represented in longitudinal-latitudinal-vertical grids. The tropospheric and stratospheric chemistry schemes are denoted as interactive (I), prescribed (P) and none (N) in "Trop" and "Strat" columns. The realisation, physics and forcing indices identify ensemble experiment members. The "Fusion" column indicates whether the simulation experiments are included into multi-model fusion. Full names of the CMIP6 participant research institutes and detailed information of coupling components of earth system models are listed in Supplementary Information.

Institute	Model	Trop	Strat	Grids	Realisations	Physics	Forcing	Fusion	Refs
AWI	**ESM**‖	P[#]	P	192×96×47	r_1[⊥]	p_1	f_1		21
BCC	**ESM1**	I	P	128×64×26	r_1, r_2, r_3	p_1	f_1	√	22, 23
	CSM2	P	P	320×160×19	r_1	p_1	f_1		24-26
CNRM[*]	**CM6.1**	N	I	256×128×91	$r_{1\text{-}5}$	p_1	f_2		27-29
	ESM2.1	N	I	256×128×91	r_1, r_2, r_3	p_1	f_2		28, 30, 31
HAMMOZ[§]	**MPI-ESM1.2-HAM**	I	P	192×96×47	r_1, r_2	p_1	f_1	√	32
IPSL	**CM6A**	P	P	144×143×79	$r_{1\text{-}10}$	p_1	f_1		33, 34
MOHC	**UKESM1-0-LL**[†]	I	I	192×144×85	$r_{10\text{-}12}, r_{14\text{-}19}$	p_1	f_2	√	
	UKESM1-0-LL	I	I	192×144×85	$r_{5\text{-}7}$	p_1	f_3	√	15, 35-39
MO-NERC	**UKESM1-0-LL**	I	I	192×144×85	$r_{1\text{-}4}, r_{8\text{-}9}$	p_1	f_2	√	
MPI-M	**ESM1.2-HR**	P	P	384×192×95	$r_{1\text{-}10}$	p_1	f_1		40-43
MRI	**ESM2.0**	I	I	128×64×80	$r_{1\text{-}5}$	p_1	f_1	√	44-46
NASA-GISS	**E2.1-G**	I	I	144×90×40	$r_{1\text{-}10}$	p_3	f_1	√	
	E2.1-G	I	I	144×90×40	r_1, r_2, r_3	p_5	f_1	√	47-49
	E2.1-H	I	I	144×90×40	$r_{1\text{-}5}$	p_3	f_1	√	
	E2.1-H	I	I	144×90×40	r_1, r_2, r_3	p_5	f_1	√	
NCAR	**CESM2-WACCM6**	I	I	288×192×70	r_1, r_2, r_3	p_1	f_1	√	50, 51
NCC	**NorESM-MM**[‡]	I	P	288×192×32	r_1, r_2, r_3	p_1	f_1	√	52
NIMS-KMA	**UKESM1-0-LL**	I	I	192×144×85	r_{13}	p_1	f_2	√	53
NOAA-GFDL	**ESM4**	I	I	288×180×49	r_1	p_1	f_1	√	54, 55

‖ The earth system models are unique for each institute, but coincidently are named the same as ESM with version numbers, thus are named by institute + model name hereafter in this paper for distinguishment (i.e. CNRM-ESM2.1 is not an updated version of BCC-ESM1, but a new version of CNRM-ESM1)[56].

[#] AWI-ESM, BCC-CSM2, IPSL-CM6A, and MPI-M-ESM1.2-HR use the same prescribed ozone for the whole earth system modelling instead of simulating the ozone, so that the surface ozone concentrations reported by these 4 models are essentially the same. In this sense, the single prescribed ozone (input4MIPs)[57] is used in place of the 4 models to avoid duplication.

[⊥] All the realisations of the climate equilibrium started since 1850, so that are marked with the same initialisation index, i_1. The ensemble experiment variant serial numbers are defined by a combination of realisation, initialisation, physics, and forcing, e.g. $r_1i_1p_1f_1$.

[*] The 2 CNRM models are not considered for surface ozone multi-model fusion as they do not include tropospheric ozone module.

[§] Full name as HAMMOZ-Consortium, marked as HAM in model name.

[†] MOHC, MO-NERC and NIMS-KMA ran the same UKESM1 model with same configuration, but contributed different ensemble experiments, so that are referred collectively as UKESM1-0-LL hereafter in this paper.

[‡] NCC ran the NorESM in two different coupling resolutions, as low atmospheric-medium ocean resolution (LM) and median atmospheric-medium ocean resolution (MM). In order to achieve higher performance in multi-model fusion, only the higher spatial-resolution simulation, MM, is considered so as to avoid duplication.

Table S2 Diagnostic features of model fitting regression for the seasonal oscillations of TOAR monthly average surface ozone concentrations. A total of 25-year 300-month observations were included in the TOAR project. The mathematical formulae were given together with abbreviated models names as index. The coefficient of determinacy (R^2), rooted mean squared error (RMSE), and Akaike Information Criteria (AIC) were calculated as model selection criteria. The temporal term t was set as the serial month since January 1990.

Model	Equation	R^2	RMSE	$k^{\dagger}$	AIC
F1-L-L‡	$\hat{y}(t) = (a_0 + a_1 t) + (b_0 + b_1 t) \times sin(\frac{\pi}{6} t + \varphi_1)$	0.9103	1.55	5	266.79
F1-L-E	$\hat{y}(t) = (a_0 + a_1 t) + (b_0 e^{b_1 t}) \times sin(\frac{\pi}{6} t + \varphi_1)$	0.9101	1.55	5	267.56
F1-E-L	$\hat{y}(t) = (a_0 e^{a_1 t}) + (b_0 + b_1 t) \times sin(\frac{\pi}{6} t + \varphi_1)$	0.9101	1.55	5	267.39
F1-E-E	$\hat{y}(t) = (a_0 e^{a_1 t}) + (b_0 e^{b_1 t}) \times sin(\frac{\pi}{6} t + \varphi_1)$	0.9099	1.55	5	268.11
F2-L-L-C	$\hat{y}(t) = (a_0 + a_1 t) + (b_0 + b_1 t) \times sin(\frac{\pi}{6} t + \varphi_1) + c_0 \times sin(\frac{2\pi}{6} t + \varphi_2)$	0.9563	1.08	7	55.41
F2-L-L-L	$\hat{y}(t) = (a_0 + a_1 t) + (b_0 + b_1 t) \times sin(\frac{\pi}{6} t + \varphi_1) + (c_0 + c_1 t) \times sin(\frac{2\pi}{6} t + \varphi_2)$	0.9565	1.08	8	55.75
F2-L-L-E	$\hat{y}(t) = (a_0 + a_1 t) + (b_0 + b_1 t) \times sin(\frac{\pi}{6} t + \varphi_1) + (c_0 e^{c_1 t}) \times sin(\frac{2\pi}{6} t + \varphi_2)$	0.9565	1.08	8	55.66
F2-L-E-C	$\hat{y}(t) = (a_0 + a_1 t) + (b_0 e^{b_1 t}) \times sin(\frac{\pi}{6} t + \varphi_1) + c_0 \times sin(\frac{2\pi}{6} t + \varphi_2)$	0.9546	1.11	7	66.77
F2-L-E-L	$\hat{y}(t) = (a_0 + a_1 t) + (b_0 e^{b_1 t}) \times sin(\frac{\pi}{6} t + \varphi_1) + (c_0 + c_1 t) \times sin(\frac{2\pi}{6} t + \varphi_2)$	0.9547	1.11	8	68.19
F2-L-E-E	$\hat{y}(t) = (a_0 + a_1 t) + (b_0 e^{b_1 t}) \times sin(\frac{\pi}{6} t + \varphi_1) + (c_0 e^{c_1 t}) \times sin(\frac{2\pi}{6} t + \varphi_2)$	0.9549	1.10	8	66.75
F2-E-L-C	$\hat{y}(t) = (a_0 e^{a_1 t}) + (b_0 + b_1 t) \times sin(\frac{\pi}{6} t + \varphi_1) + c_0 \times sin(\frac{2\pi}{6} t + \varphi_2)$	0.9564	1.08	7	54.18
F2-E-L-L	$\hat{y}(t) = (a_0 e^{a_1 t}) + (b_0 + b_1 t) \times sin(\frac{\pi}{6} t + \varphi_1) + (c_0 + c_1 t) \times sin(\frac{2\pi}{6} t + \varphi_2)$	0.9562	1.09	8	57.84
F2-E-L-E	$\hat{y}(t) = (a_0 e^{a_1 t}) + (b_0 + b_1 t) \times sin(\frac{\pi}{6} t + \varphi_1) + (c_0 e^{c_1 t}) \times sin(\frac{2\pi}{6} t + \varphi_2)$	0.9562	1.09	8	57.49
F2-E-E-C	$\hat{y}(t) = (a_0 e^{a_1 t}) + (b_0 e^{b_1 t}) \times sin(\frac{\pi}{6} t + \varphi_1) + c_0 \times sin(\frac{2\pi}{6} t + \varphi_2)$	0.9559	1.09	7	57.58
F2-E-E-L	$\hat{y}(t) = (a_0 e^{a_1 t}) + (b_0 e^{b_1 t}) \times sin(\frac{\pi}{6} t + \varphi_1) + (c_0 + c_1 t) \times sin(\frac{2\pi}{6} t + \varphi_2)$	0.9561	1.09	8	58.36
F2-E-E-E	$\hat{y}(t) = (a_0 e^{a_1 t}) + (b_0 e^{b_1 t}) \times sin(\frac{\pi}{6} t + \varphi_1) + (c_0 e^{c_1 t}) \times sin(\frac{2\pi}{6} t + \varphi_2)$	0.9561	1.09	8	58.19

† k represents the degree of freedom, which is equal to the number of parameters.

‡ The model abbreviations were defined by the order(s) of Fourier Series, and the sub-types of each term, sequenced as the intercept, 1^{st}- and 2^{nd}- order series. F1, 1^{st}-order Fourier Series models. F2, 2^{nd}-order Fourier Series models. L, linear coefficient. E, exponential coefficient. C, constant coefficient.

Table S3 Model-observation error decomposition of aggressive and conservative multi-model ensemble integration approaches for each continent. The metrics include the values and ratios of bias, root variance and root noise, summarised with arithmetic mean, median and inter-quartile range (IQR, 25-75%ile). The continental statistics are summarised based on the TOAR realistic measurement-covered sites.

			Europe		North America		South America		Asia		Africa		Oceania	
			mean (median)	*IQR*	*mean (median)*	*IQR*	*mean (median)*	*IQR*	*mean (median)*	*IQR*	*mean (median)*	*IQR*	*mean (median)*	*IQR*
Aggressive	**Value**	*Bias*	0.78 (0.63)	0.36 – 1.05	0.58 (0.49)	0.23 – 0.79	0.38 (0.17)	0.13 – 0.23	0.93 (0.47)	0.31 – 1.24	0.83 (0.63)	0.22 – 0.77	0.17 (0.17)	0.06 – 0.22
		Variance$^{1/2}$	0.80 (0.75)	0.59 – 0.92	0.57 (0.53)	0.35 – 0.74	0.73 (0.91)	0.42 – 0.95	1.02 (0.93)	0.71 – 1.27	1.27 (1.14)	1.07 – 1.43	0.46 (0.41)	0.33 – 0.56
		Noise$^{1/2}$	1.50 (1.37)	1.22 – 1.66	1.33 (1.29)	1.14 – 1.50	1.02 (1.00)	0.80 – 1.12	1.69 (1.62)	1.19 – 1.97	1.55 (1.56)	1.48 – 1.58	0.77 (0.77)	0.68 – 0.93
	Ratio	*Bias*	0.18 (0.14)	0.04 – 0.27	0.16 (0.09)	0.03 – 0.24	0.09 (0.02)	0.01 – 0.07	0.18 (0.11)	0.03 – 0.25	0.14 (0.08)	0.02 – 0.11	0.05 (0.04)	0.01 – 0.09
		Variance$^{1/2}$	0.19 (0.17)	0.12 – 0.25	0.14 (0.12)	0.06 – 0.20	0.30 (0.33)	0.17 – 0.39	0.24 (0.24)	0.09 – 0.31	0.31 (0.35)	0.22 – 0.37	0.24 (0.23)	0.15 – 0.32
		Noise$^{1/2}$	0.63 (0.66)	0.52 – 0.74	0.70 (0.71)	0.61 – 0.84	0.61 (0.59)	0.50 – 0.77	0.58 (0.58)	0.49 – 0.69	0.56 (0.63)	0.49 – 0.70	0.71 (0.75)	0.59 – 0.81
Conservative	**Value**	*Bias*	1.31 (1.22)	0.54 – 1.87	1.05 (0.88)	0.33 – 1.48	1.15 (0.60)	0.42 – 2.08	2.83 (1.96)	0.81 – 4.30	4.56 (4.56)	4.28 – 4.70	1.30 (0.76)	0.32 – 2.24
		Variance$^{1/2}$	0.51 (0.43)	0.25 – 0.66	0.43 (0.29)	0.15 – 0.64	1.39 (0.56)	0.25 – 1.55	1.30 (0.72)	0.31 – 1.61	1.27 (1.48)	1.28 – 1.57	0.24 (0.14)	0.02 – 0.53
		Noise$^{1/2}$	1.74 (1.58)	1.43 – 1.95	1.67 (1.61)	1.41 – 1.84	2.56 (2.62)	1.47 – 3.01	2.96 (2.41)	2.05 – 3.84	3.02 (2.43)	2.35 – 3.71	1.47 (1.48)	1.07 – 1.79
	Ratio	*Bias*	0.33 (0.29)	0.10 – 0.52	0.27 (0.20)	0.04 – 0.47	0.17 (0.10)	0.03 – 0.33	0.34 (0.24)	0.09 – 0.55	0.65 (0.68)	0.64 – 0.72	0.35 (0.26)	0.03 – 0.59
		Variance$^{1/2}$	0.07 (0.04)	0.01 – 0.08	0.06 (0.02)	0.01 – 0.08	0.17 (0.03)	0.02 – 0.31	0.10 (0.04)	0.01 – 0.10	0.06 (0.09)	0.04 – 0.09	0.03 (0.01)	0.01 – 0.04
		Noise$^{1/2}$	0.61 (0.59)	0.42 – 0.80	0.67 (0.71)	0.48 – 0.89	0.67 (0.84)	0.23 – 0.95	0.56 (0.56)	0.33 – 0.87	0.28 (0.26)	0.20 – 0.32	0.62 (0.70)	0.41 – 0.89

REFERENCES

1. Stouffer, R. J.; Weaver, A. J.; Eby, M., A method for obtaining pre-twentieth century initial conditions for use in climate change studies. *Climate Dynamics* **2004,** *23*, (3-4), 327-339.
2. Eyring, V.; Bony, S.; Meehl, G. A.; Senior, C. A.; Stevens, B.; Stouffer, R. J.; Taylor, K. E., Overview of the Coupled Model Intercomparison Project Phase 6 (CMIP6) experimental design and organization. *Geosci Model Dev* **2016,** *9*, (5), 1937-1958.
3. Dantas-Torres, F., Climate change, biodiversity, ticks and tick-borne diseases: The butterfly effect. *Int J Parasitol Parasites Wildl* **2015,** *4*, (3), 452-61.
4. Power, S.; Casey, T.; Folland, C.; Colman, A.; Mehta, V., Inter-decadal modulation of the impact of ENSO on Australia. *Climate Dynamics* **1999,** *15*, (5), 319-324.
5. Zhang, Y.; Wallace, J. M.; Battisti, D. S., ENSO-like interdecadal variability: 1900-1993. *Journal of Climate* **1997,** *10*, (5), 1004-1020.
6. Folland, C. K.; Renwick, J. A.; Salinger, M. J.; Mullan, A. B., Relative influences of the Interdecadal Pacific Oscillation and ENSO on the South Pacific Convergence Zone. *Geophysical Research Letters* **2002,** *29*, (13), 21-1-21-4.
7. Meehl, G. A.; Hu, A. X.; Arblaster, J. M.; Fasullo, J.; Trenberth, K. E., Externally Forced and Internally Generated Decadal Climate Variability Associated with the Interdecadal Pacific Oscillation. *Journal of Climate* **2013,** *26*, (18), 7298-7310.
8. Salinger, M. J.; Renwick, J. A.; Mullan, A. B., Interdecadal Pacific Oscillation and South Pacific climate. *International Journal of Climatology* **2001,** *21*, (14), 1705-1721.
9. Kerr, R. A., A north atlantic climate pacemaker for the centuries. *Science* **2000,** *288*, (5473), 1984-5.
10. Knight, J. R.; Folland, C. K.; Scaife, A. A., Climate impacts of the Atlantic Multidecadal Oscillation. *Geophysical Research Letters* **2006,** *33*, (17).
11. Knudsen, M. F.; Seidenkrantz, M. S.; Jacobsen, B. H.; Kuijpers, A., Tracking the Atlantic Multidecadal Oscillation through the last 8,000 years. *Nature Communications* **2011,** *2*, (1), 1-8.
12. Zhang, R.; Delworth, T. L., Impact of the Atlantic Multidecadal Oscillation on North Pacific climate variability. *Geophysical Research Letters* **2007,** *34*, (23).
13. Goes, J. I.; Saino, T.; Oaku, H.; Ishizaka, J.; Wong, C. S.; Nojiri, Y., Basin scale estimates of Sea Surface Nitrate and New Production from remotely sensed Sea Surface Temperature and Chlorophyll. *Geophysical Research Letters* **2000,** *27*, (9), 1263-1266.
14. Kushnir, Y., Interdecadal Variations in North-Atlantic Sea-Surface Temperature and Associated Atmospheric Conditions. *Journal of Climate* **1994,** *7*, (1), 141-157.
15. Sellar, A. A.; Walton, J.; Jones, C. G.; Wood, R.; Abraham, N. L.; Andrejczuk, M.; Andrews, M. B.; Andrews, T.; Archibald, A. T.; Mora, L.; Dyson, H.; Elkington, M.; Ellis, R.; Florek, P.; Good, P.; Gohar, L.; Haddad, S.; Hardiman, S. C.; Hogan, E.; Iwi, A.; Jones, C. D.; Johnson, B.; Kelley, D. I.; Kettleborough, J.; Knight, J. R.; Köhler, M. O.; Kuhlbrodt, T.; Liddicoat, S.; Linova-Pavlova, I.; Mizielinski, M. S.; Morgenstern, O.; Mulcahy, J.; Neininger, E.; O'Connor, F. M.; Petrie, R.; Ridley, J.; Rioual, J. C.; Roberts, M.; Robertson, E.; Rumbold, S.; Seddon, J.; Shepherd, H.; Shim, S.; Stephens, A.; Teixiera, J. C.; Tang, Y.; Williams, J.; Wiltshire, A.; Griffiths, P. T., Implementation of U.K. Earth System Models for CMIP6. *J Adv Model Earth Syst* **2020,** *12*, (4), e2019MS001946.
16. Bauer, S. E.; Tsigaridis, K.; Faluvegi, G.; Kelley, M.; Lo, K. K.; Miller, R. L.; Nazarenko, L.; Schmidt, G. A.; Wu, J., Historical (1850-2014) aerosol evolution and role on climate forcing using the GISS ModelE2.1 contribution to CMIP6. *J Adv Model Earth Syst* **2020,** *12*, (8), e2019MS001978.
17. Koch, D.; Jacob, D.; Tegen, I.; Rind, D.; Chin, M., Tropospheric sulfur simulation and sulfate direct radiative forcing in the Goddard Institute for Space Studies general circulation model. *J Geophys Res-Atmos* **1999,** *104*, (D19), 23799-23822.
18. Bauer, S. E.; Wright, D. L.; Koch, D.; Lewis, E. R.; McGraw, R.; Chang, L. S.; Schwartz, S. E.; Ruedy, R., MATRIX (Multiconfiguration Aerosol TRacker of mIXing state): an aerosol microphysical module for global atmospheric models. *Atmos Chem Phys* **2008,** *8*, (20), 6003-6035.
19. Lee, Y. H.; Adams, P. J., A Fast and Efficient Version of the TwO-Moment Aerosol Sectional (TOMAS) Global Aerosol Microphysics Model. *Aerosol Science and Technology* **2012,** *46*, (6), 678-689.
20. Liu, X. H.; Penner, J. E.; Herzog, M., Global modeling of aerosol dynamics: Model description, evaluation, and interactions between sulfate and nonsulfate aerosols. *J Geophys Res-Atmos* **2005,** *110*, (D18), 206-242.
21. Danek, C.; Shi, X.; Stepanek, C.; Yang, H.; Barbi, D.; Hegewald, J.; Lohmann, G., AWI AWI-ESM1.1LR model output prepared for CMIP6 CMIP historical. In Earth System Grid Federation: 2020.
22. Wu, T. W.; Zhang, F.; Zhang, J.; Jie, W. H.; Zhang, Y. W.; Wu, F. H.; Li, L.; Yan, J. H.; Liu, X. H.; Lu, X.; Tan, H. Y.; Zhang, L.; Wang, J.; Hu, A. X., Beijing Climate Center Earth System Model version 1 (BCC-ESM1): model description and evaluation of aerosol simulations. *Geosci Model Dev* **2020,** *13*, (3), 977-1005.
23. Zhang, J.; Wu, T.; Shi, X.; Zhang, F.; Li, J.; Chu, M.; Liu, Q.; Yan, J.; Ma, Q.; Wei, M., BCC BCC-ESM1 model output prepared for CMIP6 CMIP *piControl*. In Earth System Grid Federation: 2018.

24. Wu, T. W.; Lu, Y. X.; Fang, Y. J.; Xin, X. G.; Li, L.; Li, W. P.; Jie, W. H.; Zhang, J.; Liu, Y. M.; Zhang, L.; Zhang, F.; Zhang, Y. W.; Wu, F. H.; Li, J. L.; Chu, M.; Wang, Z. Z.; Shi, X. L.; Liu, X. W.; Wei, M.; Huang, A. N.; Zhang, Y. C.; Liu, X. H., The Beijing Climate Center Climate System Model (BCC-CSM): the main progress from CMIP5 to CMIP6. *Geosci Model Dev* **2019,** *12*, (4), 1573-1600.
25. Wu, T.; Yu, R.; Lu, Y.; Jie, W.; Fang, Y.; Zhang, J.; Zhang, L.; Xin, X.; Li, L.; Wang, Z., BCC-CSM2-HR: A High-Resolution Version of the Beijing Climate Center Climate System Model. *Geosci Model Dev* **2021**, *14*, (5), 2977-3006.
26. Wu, T.; Chu, M.; Dong, M.; Fang, Y.; Jie, W.; Li, J.; Li, W.; Liu, Q.; Shi, X.; Xin, X.; Yan, J.; Zhang, F.; Zhang, J.; Zhang, L.; Zhang, Y., BCC BCC-CSM2MR model output prepared for CMIP6 CMIP *piControl*. In Earth System Grid Federation: 2018.
27. Voldoire, A.; Saint-Martin, D.; Sénési, S.; Decharme, B.; Alias, A.; Chevallier, M.; Colin, J.; Guérémy, J. F.; Michou, M.; Moine, M. P., Evaluation of CMIP6 deck experiments with CNRM-CM6-1. *J Adv Model Earth Syst* **2019,** *11*, (7), 2177-2213.
28. Michou, M.; Nabat, P.; Saint-Martin, D.; Bock, J.; Decharme, B.; Mallet, M.; Roehrig, R.; Séférian, R.; Sénési, S.; Voldoire, A., Present-day and historical aerosol and ozone characteristics in CNRM CMIP6 simulations. *J Adv Model Earth Syst* **2020,** *12*, (1), e2019MS001816.
29. Voldoire, A., CNRM-CERFACS CNRM-CM6-1 model output prepared for CMIP6 CMIP. In Earth System Grid Federation: 2018.
30. Séférian, R.; Nabat, P.; Michou, M.; Saint-Martin, D.; Voldoire, A.; Colin, J.; Decharme, B.; Delire, C.; Berthet, S.; Chevallier, M., Evaluation of CNRM Earth System Model, CNRM-ESM2-1: Role of Earth System Processes in Present-Day and Future Climate. *J Adv Model Earth Syst* **2019,** *11*, (12), 4182-4227.
31. Seferian, R., CNRM-CERFACS CNRM-ESM2-1 model output prepared for CMIP6 CMIP. In Earth System Grid Federation: 2018.
32. Neubauer, D.; Ferrachat, S.; Siegenthaler-Le Drian, C.; Stoll, J.; Folini, D. S.; Tegen, I.; Wieners, K.-H.; Mauritsen, T.; Stemmler, I.; Barthel, S.; Bey, I.; Daskalakis, N.; Heinold, B.; Kokkola, H.; Partridge, D.; Rast, S.; Schmidt, H.; Schutgens, N.; Stanelle, T.; Stier, P.; Watson-Parris, D.; Lohmann, U., HAMMOZ-Consortium MPI-ESM1.2-HAM model output prepared for CMIP6 AerChemMIP. In Earth System Grid Federation: 2019.
33. Boucher, O.; Servonnat, J.; Albright, A. L.; Aumont, O.; Balkanski, Y.; Bastrikov, V.; Bekki, S.; Bonnet, R.; Bony, S.; Bopp, L., Presentation and evaluation of the IPSL-CM6A-LR climate model. *J Adv Model Earth Syst* **2020,** *12*, (7), e2019MS002010.
34. Boucher, O.; Denvil, S.; Levavasseur, G.; Cozic, A.; Caubel, A.; Foujols, M.-A.; Meurdesoif, Y.; Cadule, P.; Devilliers, M.; Ghattas, J.; Lebas, N.; Lurton, T.; Mellul, L.; Musat, I.; Mignot, J.; Cheruy, F., IPSL IPSL-CM6A-LR model output prepared for CMIP6 CMIP. In Earth System Grid Federation: 2018.
35. Archibald, A. T.; O'Connor, F. M.; Abraham, N. L.; Archer-Nicholls, S.; Chipperfield, M. P.; Dalvi, M.; Folberth, G. A.; Dennison, F.; Dhomse, S. S.; Griffiths, P. T.; Hardacre, C.; Hewitt, A. J.; Hill, R.; Johnson, C. E.; Keeble, J.; Köhler, M. O.; Morgenstern, O.; Mulchay, J. P.; Ordóñez, C.; Pope, R. J.; Rumbold, S.; Russo, M. R.; Savage, N.; Sellar, A.; Stringer, M.; Turnock, S.; Wild, O.; Zeng, G., Description and evaluation of the UKCA stratosphere-troposphere chemistry scheme (StratTrop vn 1.0) implemented in UKESM1. *Geosci Model Dev* **2020,** *13*, (3), 1223-1266.
36. Mulcahy, J. P.; Jones, C.; Sellar, A.; Johnson, B.; Boutle, I. A.; Jones, A.; Andrews, T.; Rumbold, S. T.; Mollard, J.; Bellouin, N.; Johnson, C. E.; Williams, K. D.; Grosvenor, D. P.; McCoy, D. T., Improved Aerosol Processes and Effective Radiative Forcing in HadGEM3 and UKESM1. *J Adv Model Earth Syst* **2018,** *10*, (11), 2786-2805.
37. Sellar, A. A.; Jones, C. G.; Mulcahy, J. P.; Tang, Y.; Yool, A.; Wiltshire, A.; O'connor, F. M.; Stringer, M.; Hill, R.; Palmieri, J., UKESM1: Description and evaluation of the UK Earth System Model. *J Adv Model Earth Syst* **2019,** *11*, (12), 4513-4558.
38. Tang, Y.; Rumbold, S.; Ellis, R.; Kelley, D.; Mulcahy, J.; Sellar, A.; Walton, J.; Jones, C., MOHC UKESM1.0-LL model output prepared for CMIP6 CMIP. In Earth System Grid Federation: 2019.
39. Yool, A.; Palmiéri, J.; Jones, C.; Sellar, A.; de Mora, L.; Kuhlbrodt, T.; Popova, E.; Mulcahy, J.; Wiltshire, A.; Rumbold, S. T., Spin-up of UK Earth System Model 1 (UKESM1) for CMIP6. *J Adv Model Earth Syst* **2020**, e2019MS001933.
40. Mauritsen, T.; Bader, J.; Becker, T.; Behrens, J.; Bittner, M.; Brokopf, R.; Brovkin, V.; Claussen, M.; Crueger, T.; Esch, M.; Fast, I.; Fiedler, S.; Flaschner, D.; Gayler, V.; Giorgetta, M.; Goll, D. S.; Haak, H.; Hagemann, S.; Hedemann, C.; Hohenegger, C.; Ilyina, T.; Jahns, T.; Jimenez-de-la-Cuesta, D.; Jungclaus, J.; Kleinen, T.; Kloster, S.; Kracher, D.; Kinne, S.; Kleberg, D.; Lasslop, G.; Kornblueh, L.; Marotzke, J.; Matei, D.; Meraner, K.; Mikolajewicz, U.; Modali, K.; Mobis, B.; Muller, W. A.; Nabel, J.; Nam, C. C. W.; Notz, D.; Nyawira, S. S.; Paulsen, H.; Peters, K.; Pincus, R.; Pohlmann, H.; Pongratz, J.; Popp, M.; Raddatz, T. J.; Rast, S.; Redler, R.; Reick, C. H.; Rohrschneider, T.; Schemann, V.; Schmidt, H.; Schnur, R.; Schulzweida, U.; Six, K. D.; Stein, L.; Stemmler, I.; Stevens, B.; von Storch, J. S.; Tian, F.; Voigt, A.; Vrese, P.; Wieners, K. H.; Wilkenskjeld, S.; Winkler, A.; Roeckner, E., Developments in the MPI-M Earth System Model version 1.2 (MPI-ESM1.2) and Its Response to Increasing CO_2. *J Adv Model Earth Syst* **2019,** *11*, (4), 998-1038.
41. Müller, W. A.; Jungclaus, J. H.; Mauritsen, T.; Baehr, J.; Bittner, M.; Budich, R.; Bunzel, F.; Esch, M.; Ghosh, R.; Haak, H., A Higher-resolution Version of the Max Planck Institute Earth System Model (MPI-ESM1.2-HR). *J Adv Model Earth Syst* **2018,** *10*, (7), 1383-1413.

42. Gutjahr, O.; Putrasahan, D.; Lohmann, K.; Jungclaus, J. H.; von Storch, J. S.; Bruggemann, N.; Haak, H.; Stossel, A., Max Planck Institute Earth System Model (MPI-ESM1.2) for the High-Resolution Model Intercomparison Project (HighResMIP). *Geosci Model Dev* **2019,** *12*, (7), 3241-3281.
43. von Storch, J.-S.; Putrasahan, D.; Lohmann, K.; Gutjahr, O.; Jungclaus, J.; Bittner, M.; Haak, H.; Wieners, K.-H.; Giorgetta, M.; Reick, C.; Esch, M.; Gayler, V.; de Vrese, P.; Raddatz, T.; Mauritsen, T.; Behrens, J.; Brovkin, V.; Claussen, M.; Crueger, T.; Fast, I.; Fiedler, S.; Hagemann, S.; Hohenegger, C.; Jahns, T.; Kloster, S.; Kinne, S.; Lasslop, G.; Kornblueh, L.; Marotzke, J.; Matei, D.; Meraner, K.; Mikolajewicz, U.; Modali, K.; Müller, W.; Nabel, J.; Notz, D.; Peters, K.; Pincus, R.; Pohlmann, H.; Pongratz, J.; Rast, S.; Schmidt, H.; Schnur, R.; Schulzweida, U.; Six, K.; Stevens, B.; Voigt, A.; Roeckner, E., MPI-M MPI-ESM1.2-XR model output prepared for CMIP6 HighResMIP. In Earth System Grid Federation: 2017.
44. Yukimoto, S.; Kawai, H.; Koshiro, T.; Oshima, N.; Yoshida, K.; Urakawa, S.; Tsujino, H.; Deushi, M.; Tanaka, T.; Hosaka, M.; Yabu, S.; Yoshimura, H.; Shindo, E.; Mizuta, R.; Obata, A.; Adachi, Y.; Ishii, M., The Meteorological Research Institute Earth System Model Version 2.0, MRI-ESM2.0: Description and Basic Evaluation of the Physical Component. *Journal of the Meteorological Society of Japan* **2019,** *97*, (5), 931-965.
45. Yukimoto, S.; Adachi, Y.; Hosaka, M.; Sakami, T.; Yoshimura, H.; Hirabara, M.; Tanaka, T. Y.; Shindo, E.; Tsujino, H.; Deushi, M.; Mizuta, R.; Yabu, S.; Obata, A.; Nakano, H.; Koshiro, T.; Ose, T.; Kitoh, A., A New Global Climate Model of the Meteorological Research Institute: MRI-CGCM3-Model Description and Basic Performance. *Journal of the Meteorological Society of Japan* **2012,** *90A*, 23-64.
46. Yukimoto, S.; Koshiro, T.; Kawai, H.; Oshima, N.; Yoshida, K.; Urakawa, S.; Tsujino, H.; Deushi, M.; Tanaka, T.; Hosaka, M.; Yoshimura, H.; Shindo, E.; Mizuta, R.; Ishii, M.; Obata, A.; Adachi, Y., MRI MRI-ESM2.0 model output prepared for CMIP6 CMIP. In Earth System Grid Federation: 2019.
47. Shindell, D. T.; Pechony, O.; Voulgarakis, A.; Faluvegi, G.; Nazarenko, L.; Lamarque, J. F.; Bowman, K.; Milly, G.; Kovari, B.; Ruedy, R.; Schmidt, G. A., Interactive ozone and methane chemistry in GISS-E2 historical and future climate simulations. *Atmos Chem Phys* **2013,** *13*, (5), 2653-2689.
48. NASA-GISS, NASA-GISS GISS-E2.1G model output prepared for CMIP6 ISMIP6. In Earth System Grid Federation: 2018.
49. NASA-GISS, NASA-GISS GISS-E2.1H model output prepared for CMIP6 CMIP. In Earth System Grid Federation: 2018.
50. Gettelman, A.; Mills, M. J.; Kinnison, D. E.; Garcia, R. R.; Smith, A. K.; Marsh, D. R.; Tilmes, S.; Vitt, F.; Bardeen, C. G.; McInerny, J.; Liu, H. L.; Solomon, S. C.; Polvani, L. M.; Emmons, L. K.; Lamarque, J. F.; Richter, J. H.; Glanville, A. S.; Bacmeister, J. T.; Phillips, A. S.; Neale, R. B.; Simpson, I. R.; DuVivier, A. K.; Hodzic, A.; Randel, W. J., The Whole Atmosphere Community Climate Model Version 6 (WACCM6). *J Geophys Res-Atmos* **2019,** *124*, (23), 12380-12403.
51. Danabasoglu, G., NCAR CESM2-WACCM model output prepared for CMIP6 CMIP. In Earth System Grid Federation: 2019.
52. Seland, Ø.; Bentsen, M.; Oliviè, D. J. L.; Toniazzo, T.; Gjermundsen, A.; Graff, L. S.; Debernard, J. B.; Gupta, A. K.; He, Y.; Kirkevåg, A.; Schwinger, J.; Tjiputra, J.; Aas, K. S.; Bethke, I.; Fan, Y.; Griesfeller, J.; Grini, A.; Guo, C.; Ilicak, M.; Karset, I. H. H.; Landgren, O. A.; Liakka, J.; Moseid, K. O.; Nummelin, A.; Spensberger, C.; Tang, H.; Zhang, Z.; Heinze, C.; Iversen, T.; Schulz, M., NCC NorESM2-LM model output prepared for CMIP6 CMIP historical. In Earth System Grid Federation: 2019.
53. Byun, Y.-H., NIMS-KMA UKESM1.0-LL model output prepared for CMIP6 AerChemMIP hist-piNTCF. In Earth System Grid Federation: 2020.
54. Krasting, J.; John, J.; Blanton, C.; McHugh, C.; Nikonov, S.; Radhakrishnan, A.; Rand, K.; Zadeh, N.; Balaji, V.; Durachta, J., NOAA-GFDL GFDL-ESM4 model output prepared for CMIP6 CMIP. In Earth System Grid Federation: 2018.
55. Horowitz, L. W.; Naik, V.; Sentman, L.; Paulot, F.; Blanton, C.; McHugh, C.; Radhakrishnan, A.; Rand, K.; Vahlenkamp, H.; Zadeh, N. T.; Wilson, C.; Ginoux, P.; He, J.; John, J. G.; Lin, M.; Paynter, D. J.; Ploshay, J.; Zhang, A.; Zeng, Y., NOAA-GFDL GFDL-ESM4 model output prepared for CMIP6 AerChemMIP. In Earth System Grid Federation: 2018.
56. Séférian, R.; Delire, C.; Decharme, B.; Voldoire, A.; Salas y Melia, D.; Chevallier, M.; Saint-Martin, D.; Aumont, O.; Calvet, J.-C.; Carrer, D., Development and evaluation of CNRM Earth system model–CNRM-ESM1. *Geosci Model Dev* **2016,** *9*, (4), 1423-1453.
57. Hegglin, M.; Kinnison, D.; Lamarque, J.-F.; Plummer, D., CCMI ozone in support of CMIP6 - version 1.0. In Earth System Grid Federation: 2016.